J. Fluid Mech. (1995), *vol.* 286, *pp.* 201–227
Copyright © 1995 Cambridge University Press

Dynamic simulation of the motion of capsules in pipelines

By J. FENG, P. Y. HUANG AND D. D. JOSEPH

Department of Aerospace Engineering and Mechanics and the Minnesota Supercomputer Institute, University of Minnesota, Minneapolis, MN 55455, USA

(Received 29 February 1994 and in revised form 21 September 1994)

In this paper we report results of two-dimensional simulations of the motion of elliptic capsules carried by a Poiseuille flow in a channel. The numerical method allows computation of the capsule motion and the fluid flow around the capsule, and accurate evaluation of the lift force and torque. Results show that the motion of a capsule which is heavier than the carrying fluid may be decomposed into three stages: initial lift-off, transient oscillations and steady flying. The behaviour of the capsule during initial lift-off and steady flying is analysed by studying the pressure and shear stress distributions on the capsule. The dominant mechanism for the lift force and torque is lubrication or inertia or a combination of the two under different conditions. The lift-off velocity for the ellipse in two dimensions is compared with experimental values for cylindrical capsules in pipes. Finally, the mechanisms of lift for capsules are applied to flying core flows, and it is argued that inertial forces are responsible for levitating heavy crude oil cores lubricated by water in a horizontal pipeline.

1. Introduction

In the early sixties, a group of researchers at the Alberta Research Council, Canada, were engaged in the study of transporting mixtures of immiscible liquids, such as crude oil and water, through pipelines. Extending the idea of these mixtures as multiphase systems, Hodgson & Charles (1963) proposed the concept of capsule pipelining†, which is the long-distance transportation of cylindrical solid forms suspended and driven by a fluid flow in a pipe. A series of studies carried out at the Alberta Research Council addressed various aspects of the motion of solid capsules in round pipes (cf. Brown 1987). A systemic account of the earlier work on capsule motion has been given by Govier & Aziz (1972). Subsequent research is represented by the numerous articles published in the proceedings of the International Conference on the Hydraulic Transport of Solids in Pipes sponsored by the British Hydromechanics Research Association (see, for example, Ellis 1976). The most recent and comprehensive studies of capsule pipelining have been done by Henry Liu and coworkers at the Capsule Pipeline Research Center at the University of Missouri-Columbia (Liu 1981, 1992).

A complete capsule pipeline system has many technical aspects. In this paper, we will only discuss the fluid mechanics involved in the motion of a single capsule which is heavier than the liquid flowing in a horizontal pipe. Previous observations have established the following scenario for a cylindrical capsule under the action of a liquid flow in a pipe. When the bulk liquid velocity V_b is below a certain value (called the

† One referee pointed out that the concept of hydraulic capsule pipelines originated with G. Pike in 1940.

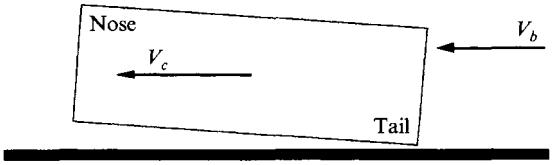

FIGURE 1. Motion of a solid capsule in a pipe: flying regime. V_b is the bulk velocity of the fluid flow (= flow rate/cross-section area), V_c is the velocity of the capsule.

incipient velocity V_i), the capsule sits still on the floor. When V_b exceeds V_i, the capsule starts to slide on the bottom, either with its side horizontal or its tail up. After V_b exceeds another threshold value (called the lift-off velocity V_L), the nose of the capsule is raised and the entire capsule becomes water-borne and 'flies' at a velocity V_c that is greater than V_b (figure 1). This flying regime is the optimal condition of operation because it consumes less power and causes less wear both on the capsule and on the pipe.

Quantities of most practical interest are the two threshold velocity values (V_i and V_L) and the holdup ratio V_c/V_b. These are affected by the following parameters: liquid velocity V_b, capsule–liquid density ratio ρ_c/ρ_f, capsule–pipe diameter ratio d/D and capsule aspect ratio d/L. The incipient velocity has been measured by a few authors, e.g. Lazarus & Kilner (1970). Liddle (1968) studied the lift-off velocity at various conditions. Ellis (1964) and Ellis & Kruyer (1970) obtained extensive data on the holdup ratio, most of which, however, fall into the sliding regime of motion. Richards' (1992) experiment covered the flying regime, but the effects of various parameters were not investigated systematically. Empirical and semi-empirical correlations have been developed based on experimental data and *ad hoc* analysis. Some of the earlier correlations were summarized by Govier & Aziz (1972). Liu's group developed a complete set of correlations that predict the incipient velocity, lift-off velocity and pressure gradient in a pipeline (Liu 1992; Richards 1992). With a large number of empirical coefficients, these relations generally work well.

So far, research work on the behaviour of a capsule in a pipeline has been mostly design-oriented. No thorough understanding of the fundamental fluid mechanics has even been attempted, especially for a capsule heavier than the carrying fluid (one exception is, perhaps, the work of Liu & Graze 1983 on the pressure distribution on a stationary capsule). Data from different experiments show conflicting trends because there is no scaling law. For example, Liddle's (1968) experiment shows that the lift-off velocity V_L increases if the diameter ratio d/D decreases. Ellis (1964) found, however, that given the same values for other parameters, capsules with smaller d/D lift off at lower liquid velocities. Analytical models are usually very rough and primitive. The main cause of these defects is that the fluid flow around the capsule is not well understood, and therefore the pressure and shear stress distribution on the capsule is completely unknown. The upshot is that the lift force and drag on the capsule have to be somehow postulated; there is then an empirical part to any 'theoretical analysis' that does not contain enough information on fluid flow around the capsule.

One particularly interesting example is the lift-off of a capsule heavier than the carrying fluid. When the liquid velocity is below V_L, the capsule slides on the bottom of the pipe, either with its side horizontal or with its tail up (Ellis 1976). This latter orientation is consistent with the pressure distribution on a stationary capsule measured by Liu & Graze (1983). If the liquid velocity exceeds V_L, the capsule

eventually adopts a nose-up orientation, and lifts off the bottom of the pipe completely. People have tried to understand the lift force that overcomes the buoyant weight of the capsule, and the mechanisms by which the nose of the capsule is kept up. Ellis (1976) attributed the lift-up of the nose to the vortex in front of the nose which creates an upward shear. The lift force was explained by an analogy to a lubricated slipper-pad (Ellis 1964). In other words, the capsule rides on a wedge of liquid which provides the support via lubrication. The lubrication mechanism does not apply to cases having large gaps and/or large tilt angles between the wall of the pipe and the bottom of the capsule. Liu (1982) attempted to interpret the lift as an inertial effect and studied the velocity profile far upstream of the capsule. The relative motion of the liquid will have a stronger impact on the bottom of the capsule than on the top. A high pressure will build under the front edge of the capsule (cf. Liu 1982, figure 2). This picture explains the nose-up orientation and also suggests a correlation for the lift force. The inclusion of inertia seems reasonable; the lift-off velocity predicted from this lift force agrees rather well with Liddle's measurement. However, the argument relies on the undisturbed relative motion of the liquid far upstream, and cannot incorporate the disturbed flow near the capsule. Thus, the physical origin of the hydrodynamic lift remains unresolved. Both Ellis (1976) and Liu (1982) recognized the importance of fluid flow near the capsule, especially at the front nose. But the characteristics of the flow have not been revealed because direct measurement is difficult.

Another example is the behaviour of a flying capsule after it lifts off. We have already noted that holdup data in the flying regime are scarce. Simplified analysis has been carried out extensively (cf. Govier & Aziz 1972). Kruyer, Redberger & Ellis (1967) assumed that the capsule is parallel to the axis of the pipe and may be eccentric. The average velocity and velocity profile in the annulus are postulated and a friction coefficient is used to estimate the drag on the capsule. The analysis of Garg (1977) allows the capsule to make an angle with the pipe wall and takes into account the solid–solid friction for a partially levitated capsule. The fundamental difficulty with this kind of analysis is that people do not understand how the capsule is suspended and tilted, and thus cannot estimate its equilibrium position and orientation in the pipe. These properties should be related to the basic parameters of the system by exploring the velocity and pressure fields around the capsule. Richards' (1992) new data on the capsule position and tilt angle are valuable as the first step toward this end.

The goal of our numerical simulation is to provide detailed information about the fluid flow around the capsule. Specifically, we will investigate the origin of the hydrodynamic lift and study the equilibrium position and orientation of a flying capsule. Our simulation is for laminar flow, but turbulence is the usual condition in applications. Another limitation of our numerical code is that only two-dimensional problems can be handled at the present time. Previous experience has proved, however, that two-dimensional simulations are able to embrace and demonstrate many important physical mechanisms in three-dimensional flow situations (Feng, Hu & Joseph 1994*a*, *b*; Huang, Feng & Joseph 1994). To avoid difficulties in programming with sharp corners, our capsule will be represented by an ellipse. A more complete dynamic simulation of all the regimes of capsule motion, including the implementation of a rectangular shape for the capsule, is currently underway, and will be reported in future publications.

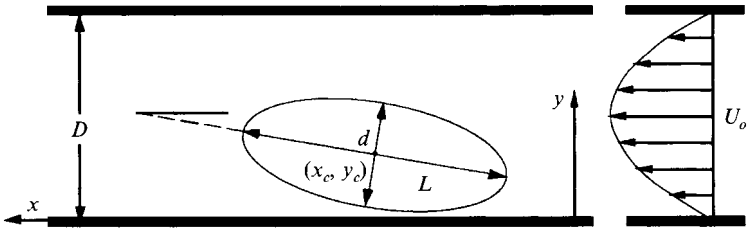

FIGURE 2. The elliptic capsule and the Poiseuille flow in a two-dimensional channel.

2. Numerical methods

Consider an elliptic capsule in a two-dimensional channel (figure 2). The width of the channel is D, and a Poiseuille flow with maximum velocity U_o prevails far upstream of the capsule. The major and minor axes of the ellipse are L and d, respectively. The centre of the ellipse is at (x_c, y_c) and its major axis makes an angle α with the direction of the undisturbed stream.

We will study the unsteady motion of the ellipse. The fluid flow is assumed to be laminar and is governed by the Navier–Stokes equations:

$$\nabla\cdot\boldsymbol{u} = 0, \qquad \frac{\partial \boldsymbol{u}}{\partial t} + \boldsymbol{u}\cdot\nabla\boldsymbol{u} = -\frac{\nabla p}{\rho_f} + \nu_f \nabla^2 \boldsymbol{u}, \tag{1}$$

where ρ_f and ν_f are the density and kinematic viscosity of the fluid. The translation and rotation of the ellipse satisfy Newton's law for rigid bodies:

$$m\frac{\mathrm{d}V}{\mathrm{d}t} = \boldsymbol{F} - m\left(1-\frac{\rho_f}{\rho_c}\right)g\boldsymbol{j}, \qquad I\frac{\mathrm{d}\boldsymbol{\Omega}}{\mathrm{d}t} = \boldsymbol{M}, \tag{2}$$

where ρ_c, m and I are the density, mass and moment of inertia of the capsule; $\boldsymbol{V}$ and $\boldsymbol{\Omega}$ are its velocity and angular velocity. $\boldsymbol{F}$ is the hydrodynamic force on the ellipse. The torque $\boldsymbol{M}$ arises as a result of the pressure and shear stress distributions on the capsule. We introduce the following non-dimensional variables:

$$\boldsymbol{x}^* = \frac{\boldsymbol{x}}{D}, \quad \boldsymbol{u}^* = \frac{\boldsymbol{u}}{U_o}, \quad t^* = \frac{U_o t}{D}, \quad p^* = \frac{p}{\rho_f U_o^2},$$

$$\boldsymbol{V}^* = \frac{\boldsymbol{V}}{U_o}, \quad \Omega^* = \frac{\Omega D}{U_o}, \quad \boldsymbol{F}^* = \frac{\boldsymbol{F}}{\rho_f U_o^2 L}, \quad \boldsymbol{M}^* = \frac{\boldsymbol{M}}{\rho_f U_o^2 L^2}.$$

Now equations (1) and (2) can be written in dimensionless forms (the asterisk has been omitted):

$$\nabla\cdot\boldsymbol{u} = 0, \qquad \frac{\partial \boldsymbol{u}}{\partial t} + \boldsymbol{u}\cdot\nabla\boldsymbol{u} = -\nabla p + \frac{1}{Re}\nabla^2\boldsymbol{u}, \tag{3}$$

$$\pi\rho\kappa_1\frac{\mathrm{d}V}{\mathrm{d}t} = \boldsymbol{F} - \pi(\rho-1)Fr\boldsymbol{j}, \qquad \frac{\pi}{4}\rho\kappa_1^2\left(\kappa_2+\frac{1}{\kappa_2}\right)\frac{\mathrm{d}\boldsymbol{\Omega}}{\mathrm{d}t} = \boldsymbol{M}, \tag{4}$$

where the dimensionless parameters are the Reynolds number $Re = U_o D/\nu_f$, the Froude number $Fr = gd/U_o^2$, the capsule–fluid density ratio $\rho = \rho_c/\rho_f$, the blockage ratio $\kappa_1 = d/D$ and the aspect ratio of the capsule $\kappa_2 = d/L$.

At $t = 0$, the ellipse is released at an initial position (x_o, y_o) with zero initial velocity. The velocity on the channel walls is zero, and the no-slip condition is applied on the surface of the capsule. The inflow boundary is $4L$ upstream of the centre of the capsule, where the Poiseuille velocity profile is assumed. The outflow boundary is $5L$

downstream of the capsule, where the normal derivatives of the velocity are put to zero. The computational domain moves with the capsule.

The Navier–Stokes equations (3) are solved using a finite element code POLYFLOW, originally developed in Belgium by the group of Professor Marcel J. Crochet (Crochet *et al.* 1991). The dynamic coupling between the fluid flow and the motion of the capsule is realized by an Explicit-Implicit scheme proposed by Hu, Joseph & Crochet (1992), which was designed for the general problem of solid particle motions. The basic procedure is as follows:

(i) Explicit updating. At each time step t_i, the current position, velocity and force of the particle are used to predict the new position and velocity at the next time step t_{i+1}.

(ii) Re-meshing and projection. For this new position, the computational domain is re-meshed, and the velocity field at t_i is projected onto the new mesh.

(iii) Navier–Stokes solution. On the new mesh, the pressure and velocity fields at t_{i+1} are solved using the velocity field at t_i (after projection). The explicitly updated particle velocity serves as the boundary condition on the particle surface. Then the force and moment on the particle are computed.

(iv) Implicit updating. The velocity of the particle is re-updated implicitly using the force and moment at t_{i+1}. If the new particle velocity is different from the one obtained in (i), then we go back to (iii) and solve the Navier–Stokes equations using the new particle velocity as the boundary condition. This process is repeated till satisfactory convergence is reached. Then we go to (i) and advance in time.

In POLYFLOW, the surface force on the solid particle is not integrated directly from the stress tensor on boundary nodes. Instead, the Gauss integral formula is used to convert this surface integral into a volume integral on the domain outside the particle. In the present paper, we are interested in the distributions of surface stresses. Therefore, the shear stress is computed directly from the velocity gradient in the finite elements around the capsule. Details of the second-order interpolation scheme are given by Huang *et al.* (1994).

The combination of POLYFLOW and the remeshing–updating method has been applied successfully to various problems of particle motion (cf. Feng *et al.* 1994*a*, *b*). Because of the strong blockage inside the channel, the capsule problem generally requires finer mesh and more grid nodes. A typical mesh has about 1500 triangular elements and 3000 nodes. Some 300 time steps are computed before the capsule attains its equilibrium position and orientation, which takes about 2 hours on a Cray-XMP supercomputer.

3. Stokes flow

Recently, Sugihara-Seki (1993) published a numerical simulation of the motion of a neutrally buoyant ellipse in a Poiseuille flow in the limit of $Re = 0$. The Stokes problem is solved for a prescribed position and orientation of the ellipse and the velocity of the ellipse is computed from the condition of vanishing force and torque. The neighbouring quasi-steady states are then connected to form the trajectory of the ellipse. Three types of periodic motion are predicted for the ellipse depending on its initial condition: (i) continuous rotation in one direction between a wall and the centreline of the channel; (ii) oscillation with its long axis swinging about $\alpha = 90°$ and its centre swinging across the centreline; (iii) oscillation with its long axis in a small-amplitude swing about $\alpha = 0°$. Type (i) occurs only when the particle is relatively small; for small particles

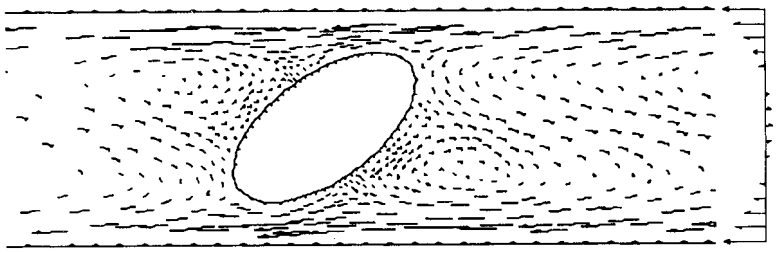

FIGURE 3. The velocity $u - V_c$ relative to the longitudinal velocity V_c of a neutrally buoyant ellipse in Stokes flow. The Poiseuille flow is from left to right. $\rho = 1$, $\kappa_1 = 0.4$, $\kappa_2 = 0.5$. Initially the ellipse is on the centreline of the channel with a tilt angle $\alpha_0 = 36°$. Dimensionless time $t = 0.26$, and the dimensionless force and torque on the ellipse are $(F_x, F_y, M_z) = (0.0589, 0.650, 0.486)$.

type (iii) occurs near the wall. For larger particles type (i) never occurs and the oscillation (iii) is on the centreline. We shall now compare our simulation in the limit of Stokes flow to the simulation of Sugihara-Seki (1993). We also wish to examine the intriguing periodic motions predicted for Stokes flow.

We set the nonlinear term $\boldsymbol{u}\cdot\nabla\boldsymbol{u}$ and the transient $\partial\boldsymbol{u}/\partial t$ to zero in equation (3). The density ratio is set to 1. Geometric parameters κ_1 and κ_2 match those used in Sugihara-Seki. A plot of the relative velocity field is shown in figure 3; this closely resembles figure 5(*a*) of Sugihara-Seki (1993) even though our capsule is not force-free and torque-free.

To study the motion of type (iii) in Sugihara-Seki's figure 13(*b*), we release a large ellipse ($\kappa_1 = 0.4472$, $\kappa_2 = 0.5$) on the centreline with $\alpha_o = 9°$. These are exactly the same initial conditions as the ones used by Sugihara-Seki except that the initial particle velocity is zero in our simulation. The trajectory and rotation of the ellipse are shown in figure 4. Shortly after the particle is released it enters an oscillation around $(y_c, \alpha) = (0.5, 0)$. The amplitude of this oscillation approaches a constant after some time. The variation in y_c and α are locked such that the major axis of the ellipse is most tilted when it is on the centreline and is parallel to the undisturbed flow when it is closest to the wall. We have essentially obtained the type (iii) oscillation described by Sugihara-Seki. However, the amplitude of y_c is about 26% smaller than that in Sugihara-Seki (1993), and the amplitude of α is 22% larger. This may be explained by one or both of the following causes. First, our simulation does not neglect the inertia of the solid particle and so it is subject to forces and acceleration. Secondly, the initial velocity is zero in our simulation and there is an initial transient. In Sugihara-Seki (1993), the 'initial velocity' is the velocity computed from the quasi-steady Stokes solution for the initial configuration, and there is no transient. In general, our code reproduces Sugihara-Seki's results in the limit of Stokes flows.

If we leave out the nonlinear term $\boldsymbol{u}\cdot\nabla\boldsymbol{u}$ but keep the transient term $\partial\boldsymbol{u}/\partial t$, the motion of the capsule is drastically different from that shown in figure 4. The capsule oscillates twice across the centreline and then approaches a steady motion on the centreline with its long axis parallel to the wall. Obviously, the transient term can be important even when $\boldsymbol{u}$ is small. A simple estimation based on the periodic motion in figure 4 shows that $\partial u/\partial t$ is some 20 times smaller than $\nabla^2 u/Re$, but $\partial v/\partial t$ can be three times larger than $\nabla^2 v/Re$. So the periodic motion of Sugihara-Seki (1993) is not physically meaningful and will not be observed in experiments. Generally, if the particle motion does not involve large accelerations and high frequencies, the quasi-static method may work well for simulations of Stokes flows (Ganatos, Pfeffer & Weinbaum 1978; Durlofsky, Brady & Bossis 1987), though the approximate trajectory is close to the true trajectory only for a finite time and the two will eventually diverge.

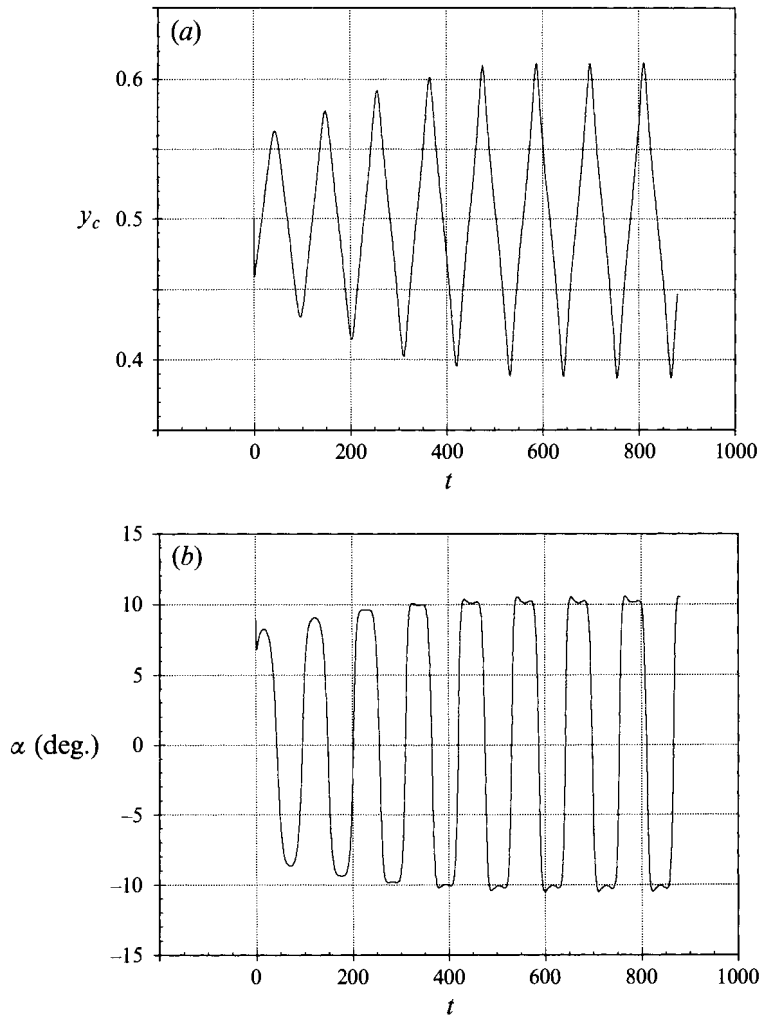

FIGURE 4. The motion of a neutrally buoyant ellipse in Stokes flow: (*a*) trajectory, (*b*) tilt angle. $\rho = 1$, $\kappa_1 = 0.4472$, $\kappa_2 = 0.5$. The ellipse was initially released on the centreline with tilt angle $\alpha_o = 9°$.

For highly transient motions, the simulation can suffer large errors even when the fluid velocity is small.

4. Results and discussion

Our major purpose in this paper is to understand the origin of the force that lifts the capsule off the floor and sustains its buoyant weight in the flying regime. The hydrodynamic forces and moment on the capsule define its motion, and in particular its position and orientation. The configuration of the capsule in turn affects the flow field around it, which then gives rise to the hydrodynamic forces and moment. This circle of events makes it difficult to launch deliberately designed test runs to isolate effects of individual factors. Hence, the mechanisms of the hydrodynamic forces and their relationship to the behaviour of the capsule are best understood by following the entire unsteady motion.

We have shown that the motion of a capsule is determined by five non-dimensional

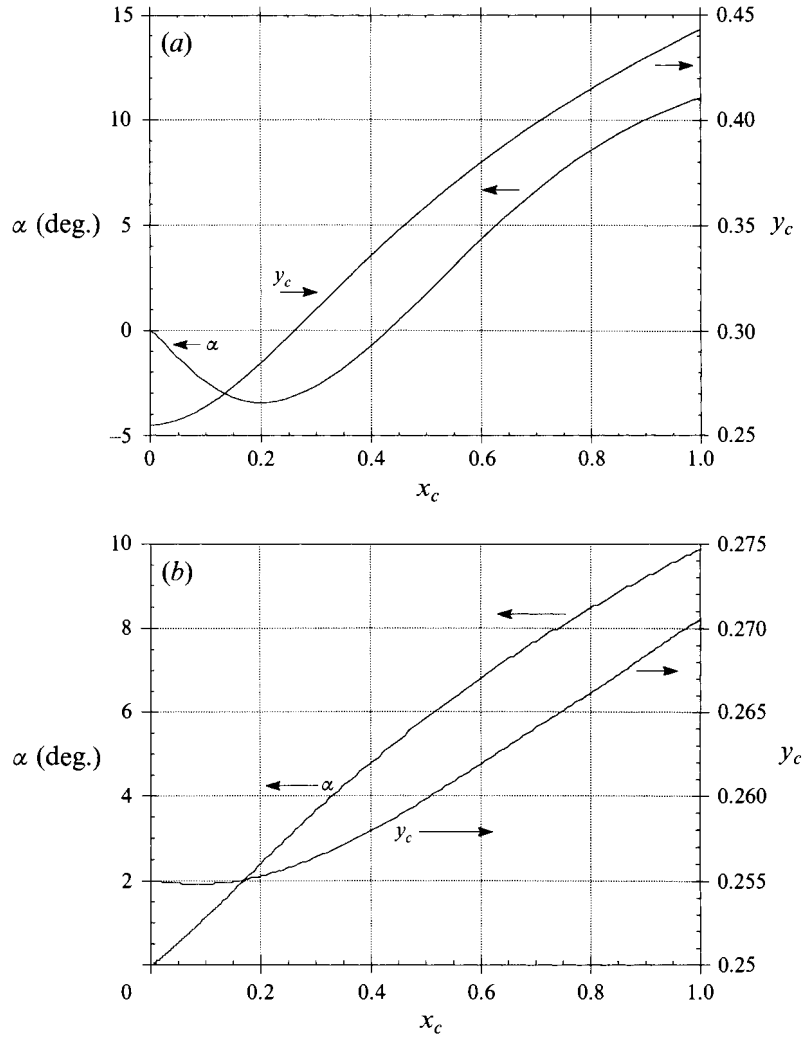

FIGURE 5. The trajectory and rotation of the capsule shortly after lift-off. $\rho = 1.01$. (*a*) $Re = 5000$, the tail lifts off first (negative α); (*b*) $Re = 250$, the nose lifts off first.

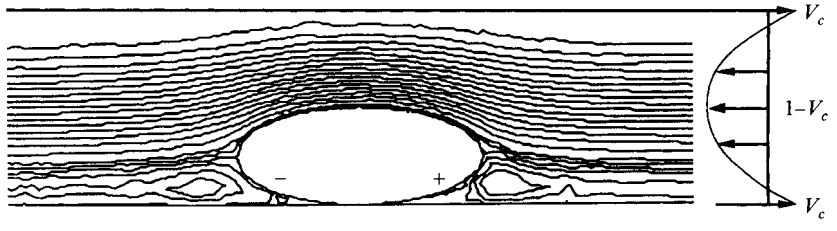

FIGURE 6. Streamlines of the relative flow around the capsule immediately after its release. $Re = 5000$, $\rho = 1.01$, time step = 3, time $t = 2.77 \times 10^{-3}$. The plus and minus sign indicate the positions of the maximum and minimum pressure.

parameters: Re, Fr, ρ, κ_1 and κ_2. In this paper, the effects of geometry are not studied and we set $\kappa_1 = 0.5$, $\kappa_2 = 0.4$ for all the computations. These values are close to those of a typical capsule pipeline (Liu 1982). An efficient way to study Re, Fr, ρ is to examine the effect of each parameter while holding the other two constant. However, none of

the experimental results in the literature has been presented in this framework. In the context of experimental research and practical operations, it is more natural to vary the fluid velocity and observe the behaviour of the capsule while other properties, such as the fluid viscosity, capsule density, its shape and size, are fixed. For example, the different regimes of motion are always described in terms of threshold velocities (Liu 1992). Here, we will follow the traditional approach of using U_0 and ρ_c as the control variables. In the computation, U_0 is represented by the Reynolds number Re and ρ_c by the density ratio ρ. We prescribe κ_1, κ_2 and $Fr\,Re^2 = gdD^2/\nu_f^2 = 4.9 \times 10^6$ while varying Re and ρ.

In most of the simulations, the capsule is released at an initial position $(x_0, y_0) = (0, 0.255)$ with the major axis horizontal. Note that the lowest point under the capsule is only 0.005 off the floor. We consider this an approximation to the situation where the capsule sits on the floor. Reducing this clearance to 0.002 does not affect the results. But a still closer approach between the wall and the capsule causes difficulties in our mesh generator and the whole code fails.

For all the ρ and Re values we have tested, the motion of the capsule can be decomposed into three stages: initial lift-off, transient bumps and steady flying. After release, the centre of the capsule starts to move forward and then upward. Depending on the magnitude of Re, the initial rotation can be in either direction, and so the capsule assumes a tail-up or nose-up posture. Then there is a transient phase when both the elevation and the orientation of the capsule oscillate. Finally the capsule attains an equilibrium position and orientation and flies steadily with its nose up. The mechanisms of lift will be studied both in the lift-off and the steady flying stages. We call attention to the fact that the term 'lift-off' is used in two senses in this paper. One is the *initial lift-off* to be discussed next; the other is associated with the *lift-off velocity* V_L, which is the minimum fluid velocity to completely float the capsule (Liu 1982). The initial lift-off is the early stage of the motion of a capsule when the fluid velocity exceeds V_L. The lift-off velocity will be discussed as related to Liu's correlation in §4.3.2.

4.1. *Initial lift-off*

For a fixed value of ρ, our simulations show that lift-off is qualitatively different at small and large Re. At large Re, the tail of the capsule lifts off first, while for relatively small Re the nose lifts off first (figure 5). These two cases will be analysed separately.

4.1.1. *Lift-off at large Re*

A typical run with $Re = 5000$ and $\rho = 1.01$ is studied. Figure 6 shows the streamlines of the relative motion around the capsule immediately after release. Because the capsule has already acquired a horizontal velocity V_c, the walls of the channel are moving to the right at V_c as seen in a reference frame fixed on the capsule. The most remarkable feature is the large eddies on the under side of the capsule.

Figure 7(*a*) shows the pressure distribution on the surface of the capsule. The maximum pressure occurs at $\theta = 40°$, and the minimum at $\theta = 140°$; both positions are marked in figure 6. This distribution is just the opposite of what one would expect from lubrication, which would produce high pressure under the nose and low pressure under the tail because the floor is sliding to the right. In fact, these pressure extrema are associated with inertia.

Let us consider the relative velocity far upstream at interesting elevations. The undisturbed Poiseuille velocity profile is

$$u = 4(1-y)\,y.$$

At this time step, the centre of the capsule is at $y_c = 0.255$, leaving a gap of 0.005

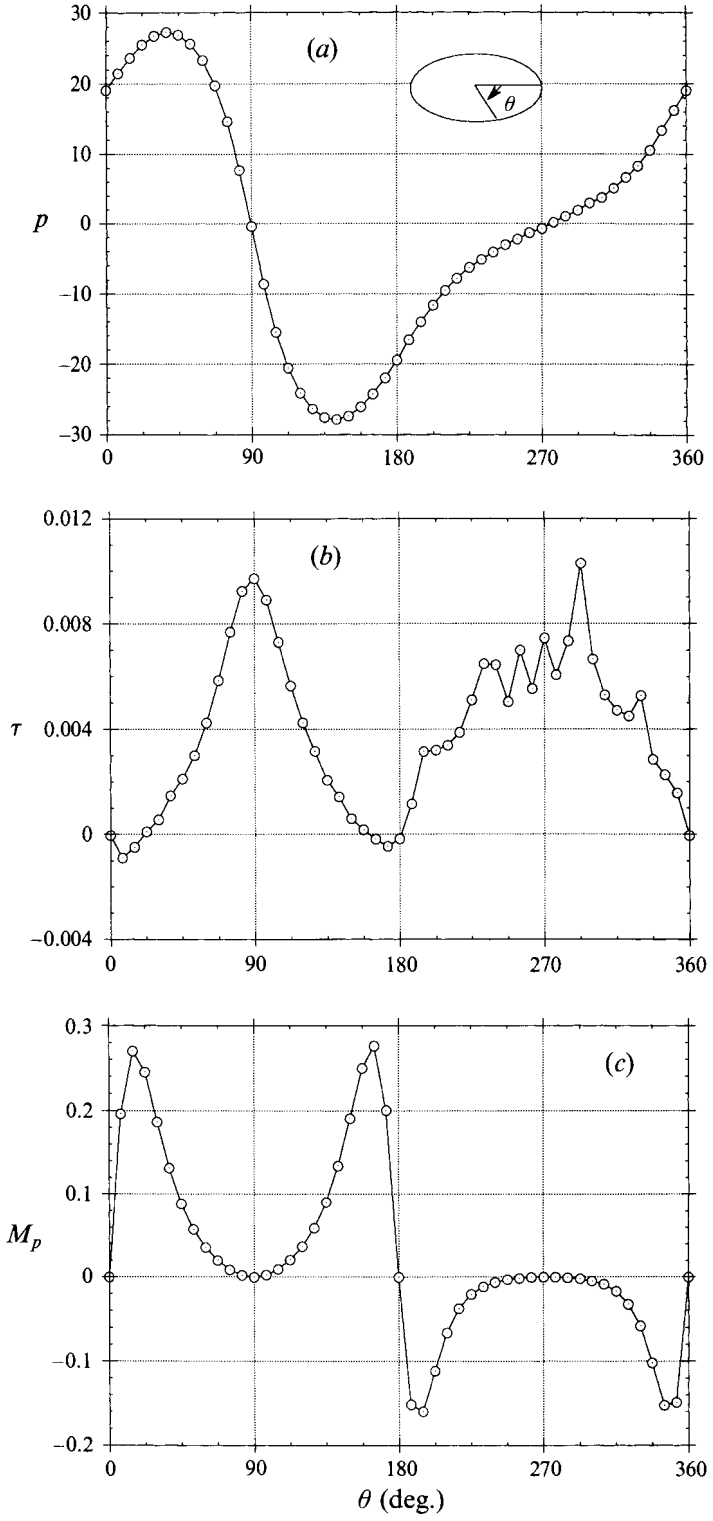

FIGURE 7. Distributions of surface stresses on the capsule. $Re = 5000$, $\rho = 1.01$, time step = 3, time $t = 2.77 \times 10^{-3}$. θ starts at the tip of the tail and goes clockwise as shown. (*a*) Pressure, made

underneath. The undisturbed velocity at the centre of the capsule is $u_c = 0.76$. The capsule velocity is $V_c = 0.265$; this means that at $y = 0.071$, the capsule feels zero relative velocity from the fluid. Therefore, immediately under the tail (say, $0° < \theta < 45°$) the flow is primarily coming from the right. This stream meets the flow entrained by the floor and a dividing streamline is created (figure 8). This gives rise to the maximum pressure under the tail. One should note that this high pressure is different from the ordinary stagnation pressure found at the front stagnation point on a solid obstacle in a stream. In the present case, two opposing streams form a compressing zone near $\theta = 50°$, where the pressure is even higher than that at the front stagnation point (around $\theta = 0°$).

Similar arguments can be applied to the minimum pressure under the nose. We again emphasize that the split streamline under the nose is different from an ordinary stagnation streamline impinging upon a solid body because of the effect of the wall. Here, the lower stream is caused by the entrainment of the floor, and the low pressure is inside an 'expansion' area stretched by diverging streams.

The shear stress distribution supports the above explanation, as τ vanishes roughly at the locations of the pressure extrema (figure 7*b*). The zeros of shear stress in a viscous fluid have been shown to correspond to the pressure extrema at the stagnation of an inviscid fluid (Huang *et al.* 1994). The pressure distribution in figure 7(*a*) produces positive torque that lifts the tail (figure 7*c*).

Finally, we note that the tail-up lift-off observed in our simulations agrees with the picture suggested by the pressure distribution measured by Liu & Graze (1983) on a stationary cylindrical capsule. In their case, the dominant feature is a negative pressure on top of the tail related to a separation bubble. This up-lift, however, is not large enough to raise the tail. Liu & Graze remarked that 'once the tail of the capsule has been lifted up by any cause, the pressure under the capsule will rise sharply and a much larger net clockwise (their flow direction is opposite to ours) moment due to lift will be generated'. This seems to be what happens in our simulation for an elliptic capsule.

4.1.2. *Lift-off at relatively small Re*

For $\rho = 1.01$ and $Re = 250$, the particle raises its nose first (figure 5*b*). The streamlines of the relative flow immediately after release are shown in figure 9. At this moment, the particle translates at $V_c = 0.569$, and the undisturbed Poiseuille velocity at the centre of the capsule is $u_c = 0.76$. Thus, the effect of the sliding motion of the floor, as compared to the effect of the Poiseuille flow at higher elevations, is much stronger than the high-*Re* lift-off in figure 6. An apparent difference is that under the nose, the circulation zone is further from the wall in figure 9 than in figure 6. This is because the floor entrains a thicker liquid layer under the nose.

The pressure and shear stress distributions (figure 10*a*, *b*) show distinct effects of viscous shear around $\theta = 90°$. The pressure variation between $\theta = 60°$ and 120° is almost exactly what one expects from lubrication theory. The high pressure under the nose and the low pressure under the tail create a large negative (clockwise) torque on the capsule (figure 10*c*) and lift the nose. The magnitudes of p and τ (scaled by ρU_o^2) are much larger for the low *Re* in figure 10 than for the high *Re* in figure 7. This loss of scaling indicates a change in the fundamental lifting mechanism. One may expect p and τ to scale linearly with U_0 at small *Re* when lubrication prevails.

dimensionless by $\rho_f U_o^2$. (*b*) Shear stress, made dimensionless by $\rho_f U_o^2$. The oscillation of τ on top of the capsule is due to numerical errors in calculating the velocity gradient. (*c*) Pressure torque M_p is computed from the pressure force on each segment of the capsule surface, clockwise torque being negative. It is made dimensionless by $\rho_f U_o^2 L^2$.

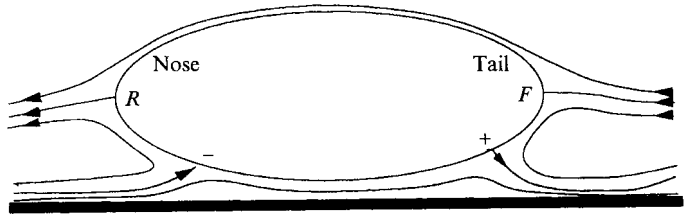

FIGURE 8. Sketch of the streamlines around the capsule. The two dividing streamlines correspond to locations of maximum and minimum pressures, which overshadow the action at the front and rear stagnation points F and R.

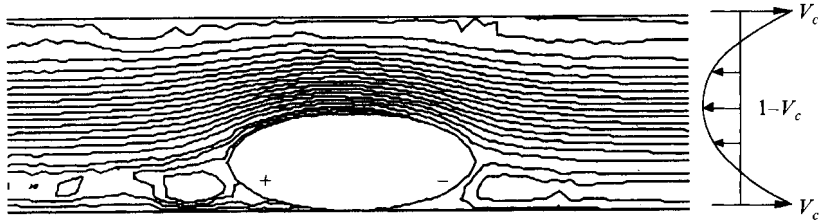

FIGURE 9. Streamlines around the capsule immediately after its release. $Re = 250$, $\rho = 1.01$, time step $= 2$, time $t = 7.5 \times 10^{-3}$. The plus and minus signs indicate the positions of the maximum and minimum pressure.

Lift-off with a nose-up posture prevails in a Re region whose upper limit is well over $Re = 250$. For $Re = 1000$, the nose still lifts off first. However, analysis of the pressure distribution indicates that lubrication and inertial effects coexist under the nose. The pressure due to entrainment rises to a maximum value as θ increases from 75° to 110°. Then there is a stagnation region between $\theta = 110°$ and 180° in which the high pressure is maintained by inertia. Both effects contribute to the upward lift and clockwise torque on the capsule.

It has been observed that long capsules tend to slide on the floor with their axes horizontal, and when the liquid velocity exceeds the lift-off velocity, the nose of the capsule lifts off first (Ellis 1964). Longer capsules have larger lift-off velocities (Liddle 1968). If a certain fluid velocity is large enough to lift a short capsule in the tail-up fashion, it may not be able to do so on a long capsule. Instead, the long capsule slides and picks up a horizontal velocity. When the relative liquid flow becomes sufficiently large under the nose, the nose will be lifted off. This is similar to the picture drawn by Liu (1982) at much higher Reynolds numbers when inertia dominates; it is also consistent with our low-Re simulation discussed here.

In summary, there is a qualitative difference between lift-off at large and small Re. At large Re, high pressure builds under the tail because of stagnation. At small Re, the stagnation pressure is not enough to lift the capsule. Instead, the fluid pushes the capsule forward until its sliding velocity is sufficiently large to produce enough lubrication lift under the nose. At somewhat higher Re, the nose-up configuration still prevails during initial lift-off, but inertial effect at the stagnation under the nose may also play a role. One may say that the Poiseuille flow in the central area of the channel dominates the flow caused by the sliding floor at high Re, and the wall-induced shear dominates the Poiseuille flow at low Re.

4.2. *Transient oscillations*

Following the initial lift-off, the capsule's elevation and tilt angle oscillate a few times before approaching its equilibrium configuration. An example of the transient

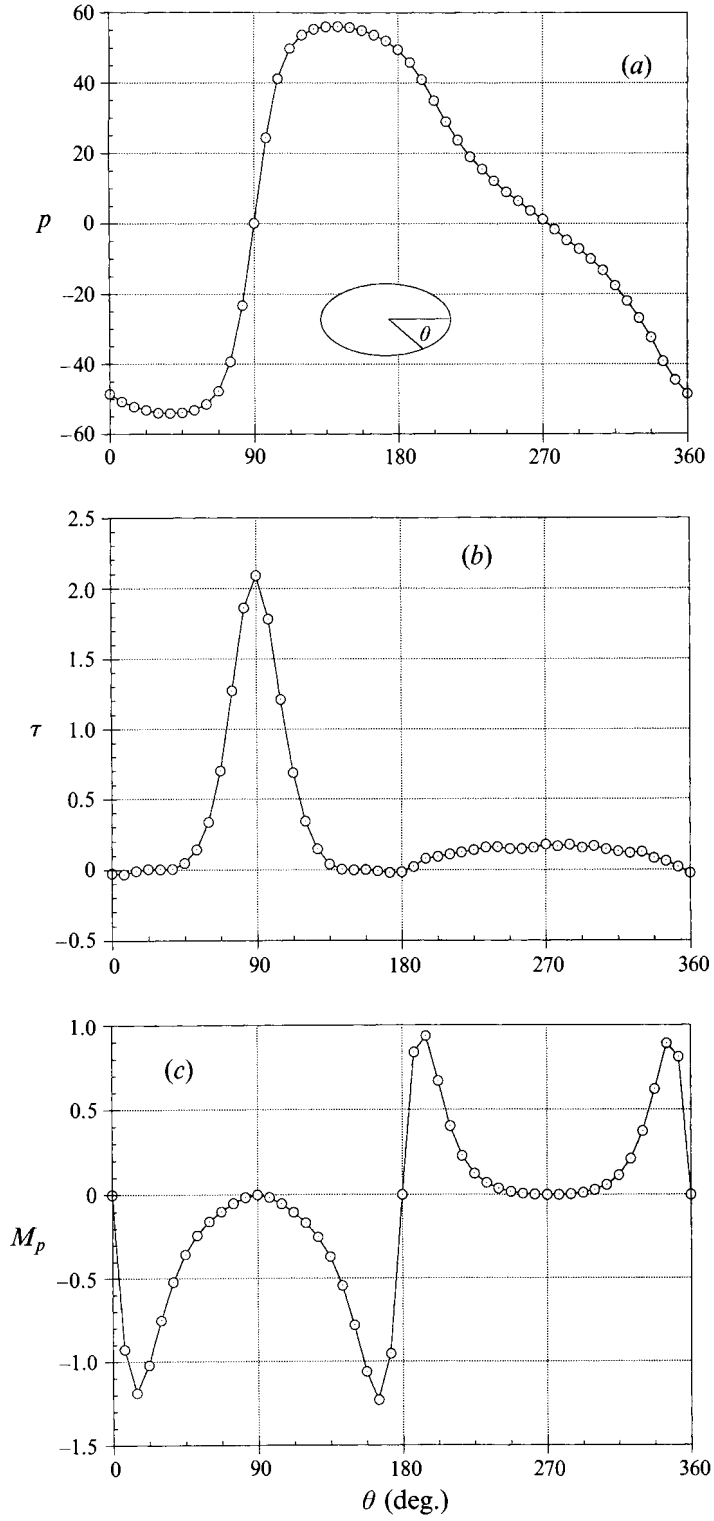

FIGURE 10. Distributions of surface stresses on the capsule. $Re = 250$, $\rho = 1.01$, time step = 2, $t = 7.5 \times 10^{-3}$. (*a*) Pressure, (*b*) shear stress, (*c*) pressure torque.

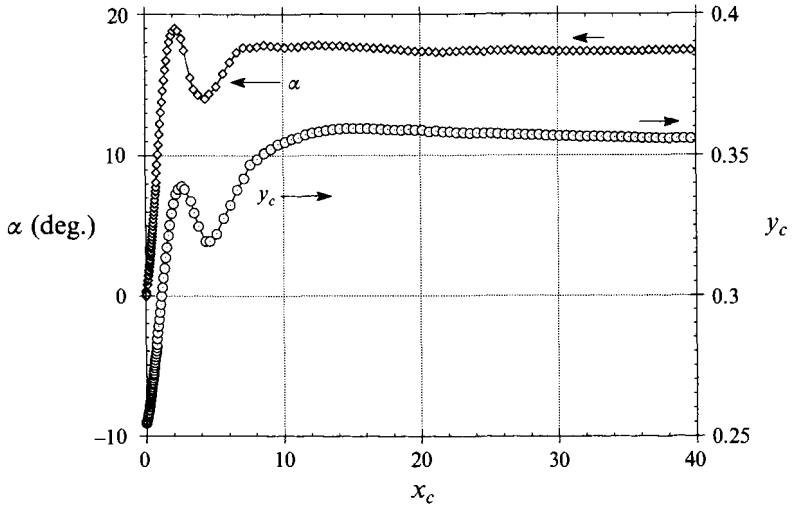

FIGURE 11. The transient bump and approach to steady flying for an elliptic capsule. $Re = 1000$, $\rho = 1.01$.

oscillations is shown in figure 11. This transient occurs for all the values of Re and ρ we have tested except for $Re = 100$ and $\rho = 1.01$, in which case the capsule approaches its final configuration without overshoot. At larger Re and/or larger ρ, the number of cycles and the amplitude of oscillation are larger.

We believe that the transient is associated with the inertia of the capsule. When first lifted, the capsule acquires a considerable upward velocity and the gap underneath becomes larger. So the hydrodynamic lift is reduced and is no longer enough to hold the buoyant weight of the capsule and it falls. This overshoot repeats while the capsule adjusts its elevation and orientation. The effects of Re and ρ on the transient support this argument based on the inertia of the capsule. The force and torque balance that establishes the steady flying as the transient subsides will be studied next.

4.3. *Steady flying*

In this regime, the equilibrium elevation y_e and tilt angle α_e are functions of Re and ρ. Figure 12(*a*) shows the effect of Re for a capsule of density $\rho = 1.01$. Figure 12(*b*) shows the effect of changing ρ at a fixed flow Reynolds number $Re = 1000$. In both plots, we notice that the variation of y_e is monotonic. A lighter capsule carried by a faster flow always assumes a higher elevation in the channel. The tilt angle α_e, however, exhibits complex patterns of variation. This suggests that under different conditions, the mechanisms of hydrodynamic forces and moment are different. Considering the effects of the channel walls and the velocity gradient, we naturally seek to identify the hydrodynamics with the elevation of the capsule. The orientation then changes as a result of the torque.

4.3.1. *Flying at low elevations*

The ellipse flies at low elevations for small Re and/or large ρ. We will analyse a typical run with $Re = 1000$ and $\rho = 1.02$. The streamlines of the relative flow are shown in figure 13. The velocity of the capsule is $V_c = 0.647$, and the flow over the top of the ellipse is mostly from right to left. The area underneath, however, is dominated by the sliding floor. Therefore, one may expect strong lubrication near the nadir. The pressure

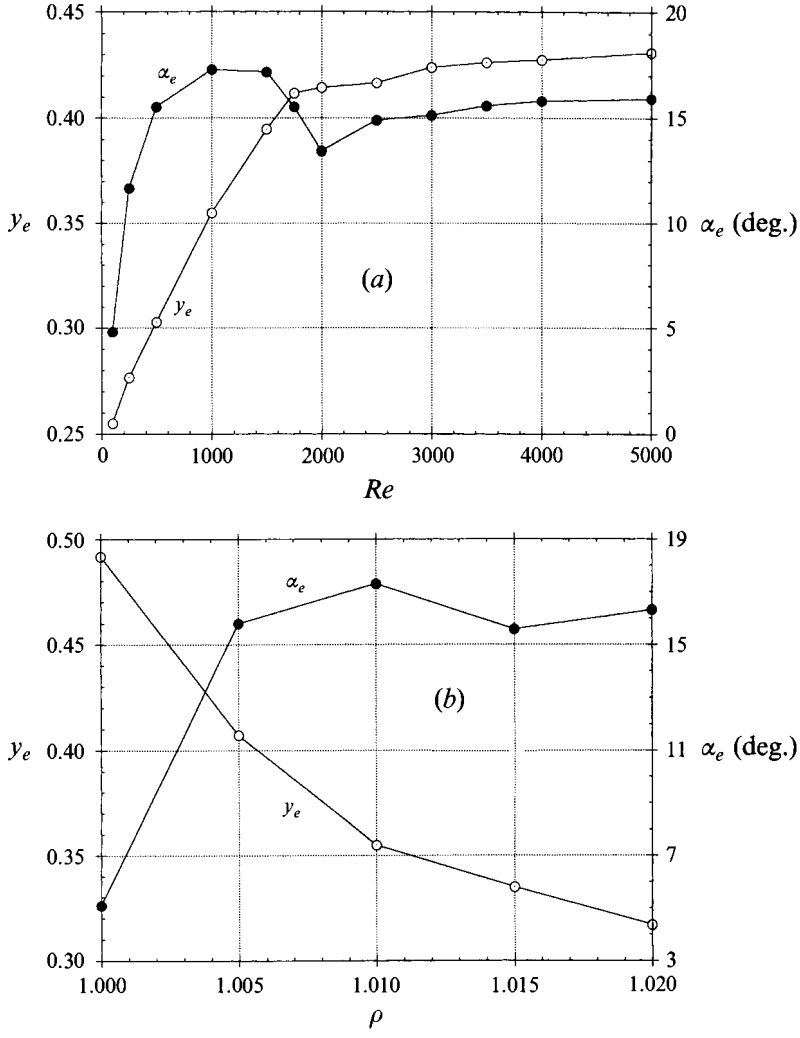

FIGURE 12. (*a*) The effect of *Re* on the elevation and orientation of the capsule in the steady flying regime. The density of the capsule is $\rho = 1.01$. (*b*) The effect of ρ on the elevation and orientation of the capsule in the steady flying regime. The Reynolds number of the fluid flow is $Re = 1000$.

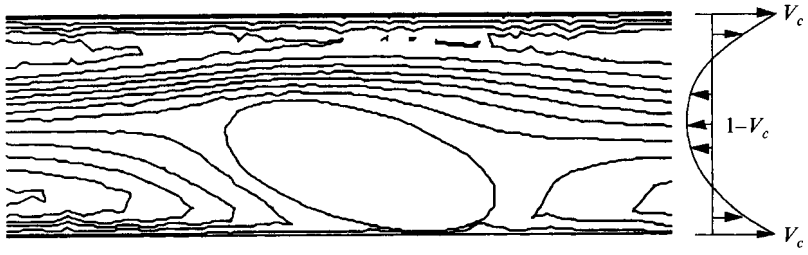

FIGURE 13. Streamlines around the capsule in steady flying. $Re = 1000$, $\rho = 1.02$, time step = 460, $t = 97.23$.

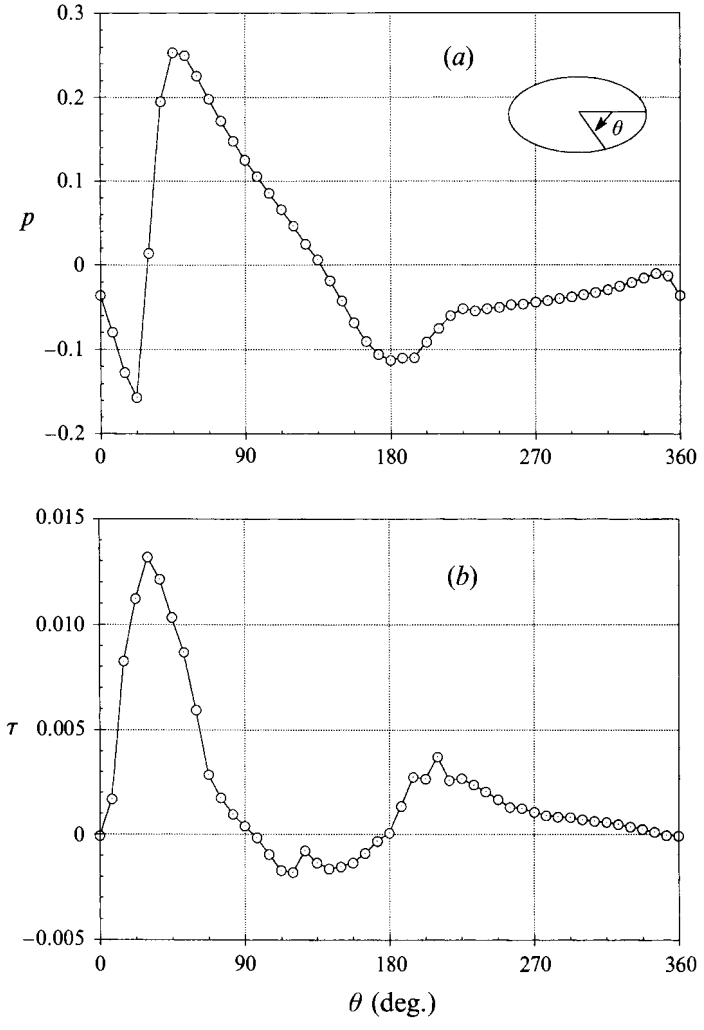

FIGURE 14. Distributions of surface stresses on the capsule. $Re = 1000$, $\rho = 1.02$, time step = 460, $t = 97.23$. (*a*) Pressure, (*b*) shear stress.

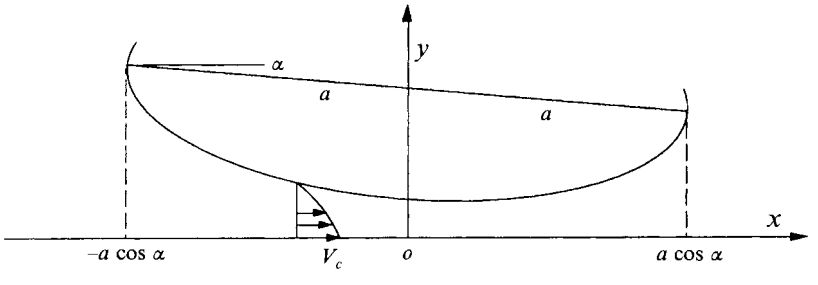

FIGURE 15. Lubrication approximation. We assume that the streamlines are nearly parallel in the gap and there is no secondary flow.

distribution (figure 14*a*) does seem to confirm this, as p changes drastically from $\theta = 22.5°$ to $\theta = 45°$. This area is close to the lowest point of the capsule where the shear stress has a maximum (figure 14*b*). Hence, the high pressure directly below the centre of the capsule must be caused by lubrication. The maximum pressure does not occur

at the stagnation point under the nose ($\theta \approx 100°$), and so is not caused by inertia. We notice the negative pressure on top of the capsule ($180° < \theta < 360°$) associated with the high velocity in the blocked region in the channel (a Bernoulli effect). This also contributes to the lift.

A simple analysis of the lubrication effect can be carried out using the method of Reynolds (see Batchelor 1988, p. 219). Let us hold the capsule fixed in space so that the floor is sliding to the right at speed V_c (figure 15, we use dimensional variables in the following derivation). We consider the bottom of the capsule between $-a\cos\alpha$ and $a\cos\alpha$. If the characteristic gap size H and the tilt angle α are small such that $\alpha V_c H/\nu_f \ll 1$, the velocity profile in the passage can be approximated by a superposition of a Couette flow and a Poiseuille flow:

$$u = -\frac{1}{2\mu_f}\frac{\mathrm{d}p}{\mathrm{d}x}y(h-y) + V_c\frac{h-y}{h},$$

The flow rate is

$$Q = \int_0^{h(x)} u(x,y)\,\mathrm{d}y = -\frac{h^3}{12\mu_f}\frac{\mathrm{d}p}{\mathrm{d}x} + \frac{V_c h}{2}$$

so that the pressure gradient can be expressed by Q and V_c:

$$\frac{\mathrm{d}p}{\mathrm{d}x} = \frac{6\mu_f V_c}{h^2} - \frac{12\mu_f Q}{h^3}.$$

Setting $p(-a\cos\alpha) = 0$, we have

$$p(x) = 6\mu_f V_c\int_{-a\cos\alpha}^{x}\frac{\mathrm{d}x}{h^2(x)} - 12\mu_f Q\int_{-a\cos\alpha}^{x}\frac{\mathrm{d}x}{h^3(x)} = 6\mu_f V_c f(x) - 12\mu_f Q g(x).$$

Because of the flow around the capsule inside the pipeline, there is a pressure difference $\delta_p = p\,(a\cos\alpha) - p(-a\cos\alpha)$. This determines the flow rate in the passage:

$$Q = \frac{V_c}{2}\frac{\delta_f}{\delta_g} - \frac{\delta_p}{12\mu_f\delta_g},$$

where $\delta_f = f(a\cos\alpha) - f(-a\cos\alpha)$, $\delta_g = g(a\cos\alpha) - g(-a\cos\alpha)$. Now the pressure distribution is

$$p(x) = 6\mu_f V_c\left[f(x) - \frac{\delta_f}{\delta_g}g(x)\right] + \frac{\delta_p}{\delta_g}g(x). \tag{5}$$

The first part of this pressure distribution is proportional to V_c and is due to the moving wall. The second part is caused by the global flow in the pipeline.

Because of the algebraic complexity in $h(x)$, we compute $f(x)$ and $g(x)$ numerically. We use the geometrical parameters of the run with $\rho = 1.01$ and $Re = 250$ in equation (5) and compare the result with the pressure obtained from direct simulation (figure 16). In this case, $(\delta_p/\delta_g)g(x)$ only makes up 0.9% of the pressure p. So wall-induced motion is indeed the dominant mechanism. The variation of pressure near $\theta = 35°$ is similar in both results. The magnitudes of the pressure extrema predicted by the lubrication theory are about 50% larger than those obtained from direct simulation. Possible causes of the discrepancy are the error intrinsic to the lubrication approximation and the limited resolution of the numerical solution. Surprisingly, the upward lift integrated from the lubrication pressure $p(x)$ is only 4% higher than the buoyant weight of the capsule.

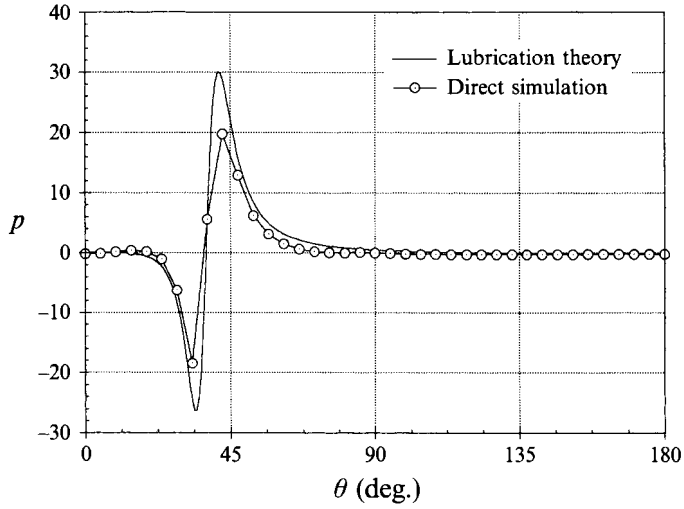

FIGURE 16. Comparison of the pressure distributions obtained by the lubrication theory and the direct simulation. $Re = 250$, $\rho = 1.01$. p is made dimensionless by $\mu_f V_c/H$, H being the minimum gap under the nadir.

Unlike the slider plate, our elliptical capsule has a curved surface and its tangent makes a variable angle with the floor. To be definite, we shall use the tilt angle α between the major axis and the ground in checking the criterion $\alpha V_c H/\nu_f \ll 1$. For $Re = 100$, 250, 500 and 1000 in figure 12(*a*), the parameter $\alpha V_c H/\nu_f$ assumes the following values: 1.133×10^{-3}, 2.261×10^{-2}, 0.7522 and 11.54. Here H is taken to be the minimum gap beneath the nadir of the capsule. In addition, the lift obtained by integrating the pressure p is of the same order of magnitude as the buoyant weight only for $Re = 100$ and 250. Thus we may say that the lubrication theory applies only to the first two points in figure 12(*a*). In this lubrication regime, if we keep the buoyant weight of the capsule constant and increase Re, the velocity of the capsule V_c increases linearly with U_o. Then the lift increases linearly and raise the elevation. The increase in the tilt angle α in figure 12(*a*) cannot be explained by the pressure caused by lubrication. Comparison of the pressure on the back of the capsule ($180° < \theta < 360°$) at different Reynolds numbers shows that at higher fluid velocity, the positive pressure above the tail of the capsule is larger in magnitude and turns the capsule clockwise. The increase in V_c, α and h work together to maintain the same lift. In figure 12(*b*), α tends to increase when ρ changes from 1.015 to 1.02. This may be associated with the fact that more lift needs to be generated at the same U_o.

If Re is further increased in figure 12(*a*), inertia becomes important. But the lubrication mechanism still exists in an area around the nadir of the ellipse. In both lubrication and inertial mechanisms, we expect the lift to increase with Re but decrease with H. So the elevation increases monotonically with Re. The change in α reflects the complex details of the pressure distribution in the transition between lubrication- and inertia-dominated regimes, and an explanation is not available. The inertial regimes at still higher Re will be studied next.

4.3.2. *Flying at high elevations*

A capsule flies at high elevations if Re is very large or ρ is very small. The tilt angle α_e, however, varies differently under the two conditions. If Re increases for a moderate ρ, α_e increases and the capsule becomes more tilted (see figure 12*a*). On the other hand,

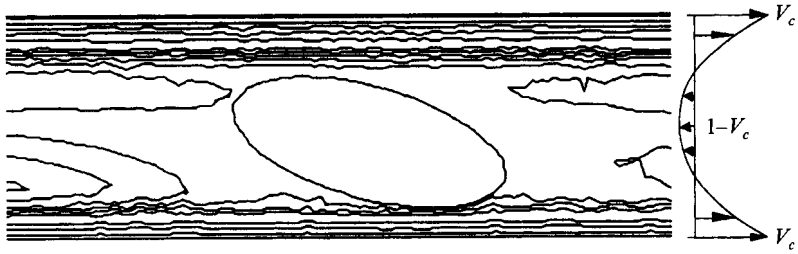

FIGURE 17. Streamlines around the capsule flying at high elevation. $Re = 5000$, $\rho = 1.01$, time step = 351, $t = 379.5$.

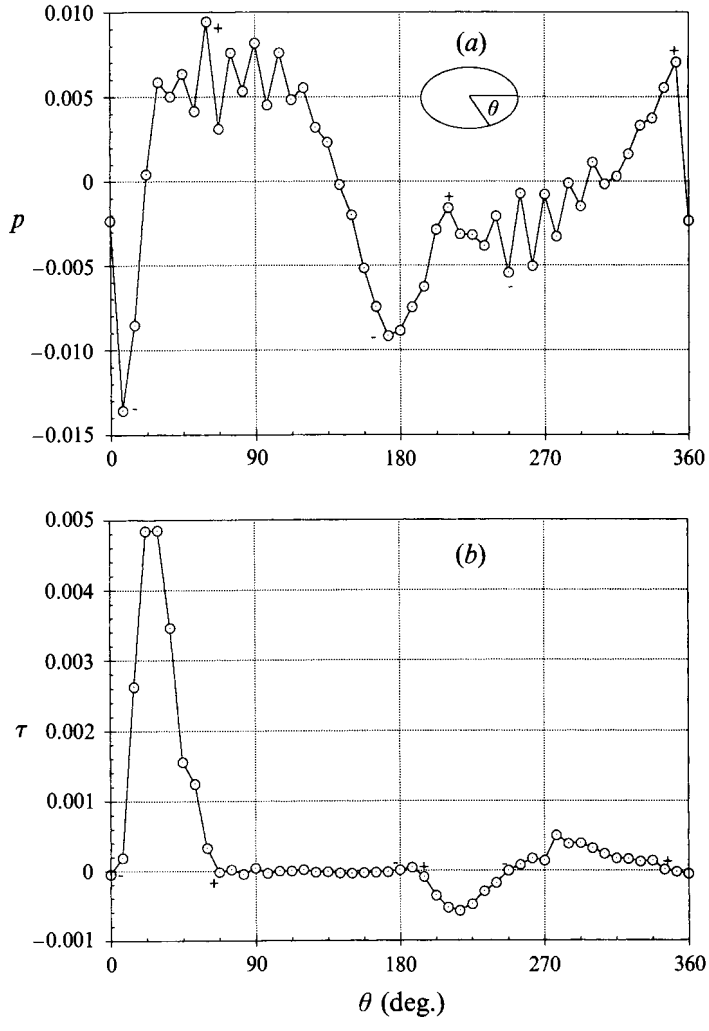

FIGURE 18. Distributions of surface stresses on the capsule in the steady flying regime. $Re = 5000$, $\rho = 1.01$, time step = 351, $t = 379.5$. (*a*) Pressure. The oscillation in p is caused by numerical errors. (*b*) Shear stress; stagnation points with high and low pressures are marked by plus and minus signs, which should also be zeros of τ. These points are less obvious in the area below and around the nose because the relative flow is weak there.

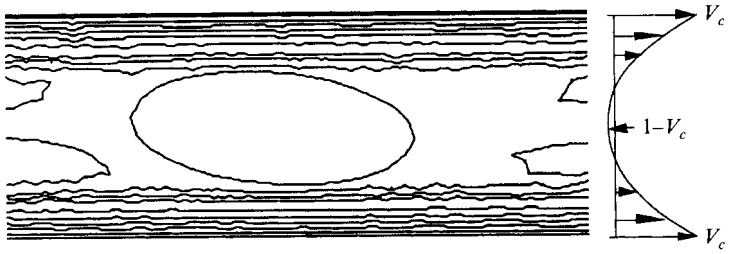

FIGURE 19. Streamlines around a capsule with zero buoyant weight. $Re = 1000$, $\rho = 1$, $V_c = 0.877$, time step = 242, $t = 144.5$.

if ρ is decreased for a fixed Re, α_e decreases and the capsule becomes more aligned with the flow (figure 12*b*). Because of the large gap between the capsule and the floor, lubrication effects are expected to be small. Two extreme cases, with $Re = 5000$, $\rho = 1.01$ and $Re = 1000$, $\rho = 1.0$ will be analysed.

For the first case, figure 17 shows six dividing streamlines and therefore six stagnation points on the surface of the capsule. These correspond to the zeros of the shear stress, which are also positions of pressure extrema (figure 18). The maximum pressure at $\theta = 60°$ gives rise to the upward lift that balances the buoyant weight. This shows that inertia is the major agent for the lift force. Comparing figure 18(*a*) to figure 14(*a*), we see that the position of maximum pressure underneath is moved toward the nose, and the stagnation pressure above the tail ($\theta \approx 348°$) becomes more important. These two differences suggest that the capsule will tilt more as U_o increases.

The other case with vanishing buoyant weight is intrinsically different because smaller and smaller lift forces are required as $\rho \to 1$. The streamlines are shown in figure 19. With the capsule centre slightly below the centreline of the channel, the flow field is almost symmetric above and below the capsule, again with six stagnation points. This near-symmetry is also reflected in the pressure and shear stress distributions around the capsule (figure 20). The fact that the pressure extrema are stronger on the underside than on the back is because the centre of the capsule is below the centreline, and thus the underside feels a stronger flow from left and right.

Since gravity is removed, $(y_e, \alpha_e) = (0.5, 0)$ is an equilibrium configuration owing to symmetry. But it is not a stable one. We have confirmed this by releasing the capsule initially on the centreline and near the upper wall. In both runs, it stabilizes a little away from the centreline with a small tilt angle (see figure 12*b*). This seems to be related to the locations of pressure extrema. If a long body on the centreline is turned slightly by a disturbance, the stagnation point under the nose (near $\theta = 112.5°$ in figure 20*a*) will turn it further. This mechanism is very much like the turning couple on a sedimenting long body (Huang *et al.* 1994), only here the low pressure above the tail keeps the capsule from turning its broadside all the way to perpendicular to the stream. Instead, the ellipse takes on a stable tilt angle and an equilibrium position that is slightly off the centreline. The effect of inertia is obvious if we recall that the symmetric configuration of $y_e = 0.5$, $\alpha_e = 0$ is stable when $\boldsymbol{u} \cdot \nabla \boldsymbol{u}$ is omitted from the Navier–Stokes equation (see §3). In summary, the tilt angle of a capsule decreases as its buoyant weight approaches zero, because very little lift is needed to support the capsule. For a neutrally buoyant capsule, the stable equilibrium tilt angle is not zero.

In the analysis of the initial lift-off and steady flying of the capsule, we have focused on extreme cases and tried to identify the hydrodynamic mechanisms at work. In all the situations between these extremes, we expect co-existence of inertial and lubrication

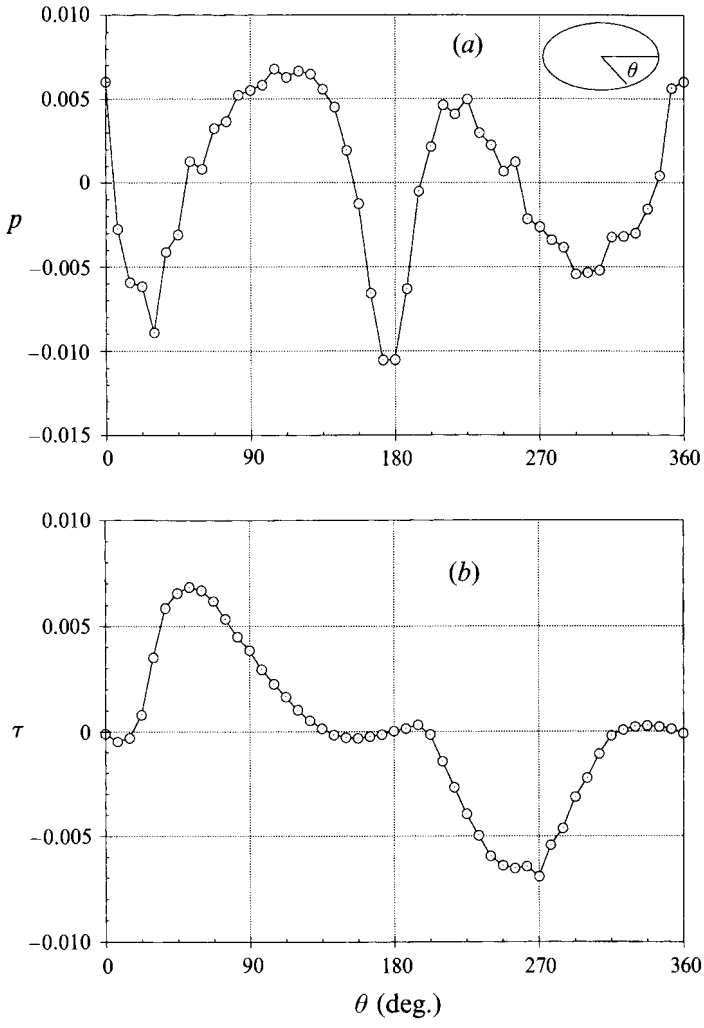

FIGURE 20. Distributions of surface stresses on the capsule in the steady flying regime. $Re = 1000$, $\rho = 1$, $V_c = 0.877$, time step = 242, $t = 144.5$. (*a*) Pressure, (*b*) shear stress.

effects and a smooth transition of relative importance between the two. The non-monotonic variations of the tilt angle α_e (around $Re = 2000$ in figure 12*a* and $\rho = 1.015$ in figure 12*b*) cannot be explained based on the available information and more detailed data are required. However, our computed results giving the variation of clearance and tilt angle are the first reported. The only experimental data comparable to our results is, to our knowledge, in the thesis of Richards (1992). Because of the difference in the Reynolds number, the Froude number, the geometry of the capsule and the fact that the simulation is in two dimensions, direct comparison with his experiment is difficult. But the qualitative behaviour is the same at high flow rate, when both y_e and α_e increase with U_o.

If we go to the limit of low flow rate, we may examine the concept of lift-off velocity. In experiments, the capsule (usually with flat ends, such as a coal log) experiences sliding, partial lifting ('micro-lift') and complete lifting ('macro-lift') as the fluid velocity increases. During micro-lift, the capsule is a small distance above the ground with a small tilt angle, and frequent solid contacts exist. The lift-off velocity is defined

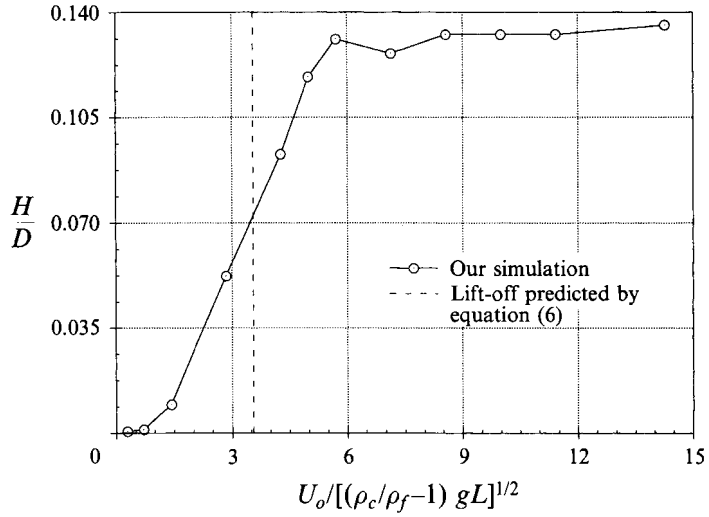

FIGURE 21. The clearance of the capsule at different fluid velocities. The abscissa is a dimensionless velocity suggested by Liu's correlation. The dashed line is twice the value given in equation (6) because V_L is the average velocity in the pipe and U_o is the maximum.

as the fluid velocity at which the clearance beneath the capsule increases sharply (Liu 1982). Our numerical program does not contain the dry friction and capsule–wall collision, and cannot simulate the transition from micro-lift to macro-lift. In fact, because our elliptic capsule has two natural wedges below its nose and tail, it can be floated by lubrication at very low fluid speed. This motion is similar to the micro-lift observed in experiments, but of different physical nature; the mechanism for micro-lift is not yet completely clear. Ellis (1976) proposed vortical motion in front of the nose that provides upward shear, and Liu (1982) suggested microscopic lubrication films related to surface roughness.

We may parallel the experiments by defining the lift-off velocity V_L in our simulation as the point where the clearance H starts to increase sharply with fluid speed U_o. From figure 21, this point can be roughly taken as $U_o/[(\rho_c/\rho_f-1)gL]^{1/2} = 1$, which is about 1/4 of the value predicted by the correlation that Liu (1982) proposed for a cylindrical capsule in a round pipe:

$$V_L = 7.2\left[\left(\frac{\rho_c}{\rho_f}-1\right)gL\left(1-\frac{d^2}{D^2}\right)\right]^{1/2}. \tag{6}$$

This correlation has proved to be quite accurate for Richards' experiment. The discrepancy between our lift-off velocity and that obtained in experiments can be explained by the following reasons. An important difference is in the shape of the capsule. The geometry of an elliptic capsule is more conducive to lubrication under its nose. Besides, our simulation is two-dimensional, and in three-dimensional experiments the fluid can go around the capsule along its sides and produce less lift. Finally, turbulence in the fluid flow in the experiment may also be a factor.

The use of elliptic capsules in our computations is good for illustrating the mechanisms of hydrodynamic lift, but is not appropriate in simulating the lift-off of a cylindrical capsule. Our results suggest that using capsules of an ellipsoidal shape may be advantageous in industrial applications. Simulations using rectangular capsules are being pursued to compare one shape with another.

The simulations presented here cover only a few aspects of capsule motion. Further work on the lift-off velocity is necessary to explore its dependence on various control parameters (cf. Ellis 1964 and Liu 1982). Effects of geometric parameters, such as the aspect ratio of the capsule d/L and the blockage ratio in the channel d/D, on the general behaviour of a capsule also need systematic study. All these issues will be discussed in a future publication.

5. Levitation of core flows†

The levitation of capsules by inertia suggests that a similar mechanism may also work in the lubrication of slurries and viscous oils in water. The viscous material does not touch the wall. In the case of crude oil, the drag reduction which can be achieved by lubrication is of the order of the viscosity ratio with increased throughputs of ten thousand or more (for more background see Joseph & Renardy 1993). These lubricated flows are called core flows because the viscous material flows in a core lubricated all around by water.

A surprising property is that core flow in a horizontal line will levitate off the wall whether the core is lighter or heavier than lubricating water. This levitation could not take place without a hydrodynamic lifting action due to waves sculpted on the core surface. In the case of very viscous liquids, the waves are basically standing waves which are connected with the core as it moves downstream. This picture suggests a lubrication mechanism for the levitation of the core analogous to mechanisms which levitate loaded slider bearings at low Reynolds numbers. Ooms *et al.* (1984) and Oliemans & Ooms (1986) gave a semi-empirical model of this type and showed that it generated buoyant forces proportional to the first power of the velocity to balance gravity. In this theory, the shape of the wave must be given as empirical input.

Another possibility which is suggested by the study of levitation of capsules is that the levitation is due to lift forces generated by inertia. Liu's (1982) formula (equation (6)) for capsule lift-off in a pipeline in which the critical lift-off velocity is proportional to the square root of gravity times the density difference is an inertial criterion. It is likely that inertial dynamics is also involved in lubricated oil and slurry lines. At high speeds the core flows may literally 'fly' down the tube.

The unsolved problem of start-up and lift-off of a stratified flow involves the levitation mechanisms under discussion. In all of this, as in the analysis of the flight of capsules and the problem of migration of particles across streamlines, the position of the viscous points of stagnation where the pressures are high is of critical importance.

We have already mentioned that a heavy or light core flow without waves cannot be levitated. Such a core will rise or fall to a wall where it will stratify. When there are no waves to corrugate the surface, the axis of the core and all the straight line generators of the core interface are parallel to the pipe and no hydrodynamic mechanism of levitation can develop. It is obvious, but not so easily proved (Hesla, Huang & Joseph 1993), that the net force and moment on the core due to interfacial tension are zero. When the densities of the oil and water are the same, the perfectly uniform core concentric with the pipe can be stable, if the parameters are in a certain small window (Joseph & Renardy 1993). This stability window also contains uniform eccentric cores, whose straight generators are parallel to the pipe wall (Huang & Joseph 1995). There is a great non-uniqueness with all kinds of eccentric core flows in the stable window and no centring mechanism can be found in the linear theory of stability.

† This section was prepared by D. D. Joseph.

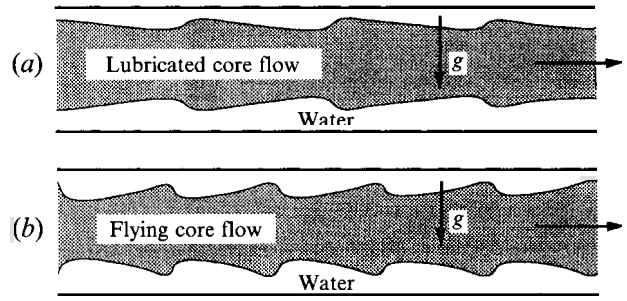

FIGURE 22. Levitation of heavy oil in water. (*a*) Saw-tooth waves arising from lubrication theory, like slider bearings. Ooms *et al.* (1984) gave a semi-empirical theory of this type (see their figure 2) and showed that it generated buoyant forces to balance gravity. Oliemans *et al.* (1985) extended this work to include the effects of turbulence in the water film, but the theory underpredicted the pressure. They said that inertia might explain the discrepancy. (*b*) Saw-tooth waves due to inertia, giving rise to aerodynamic lift.

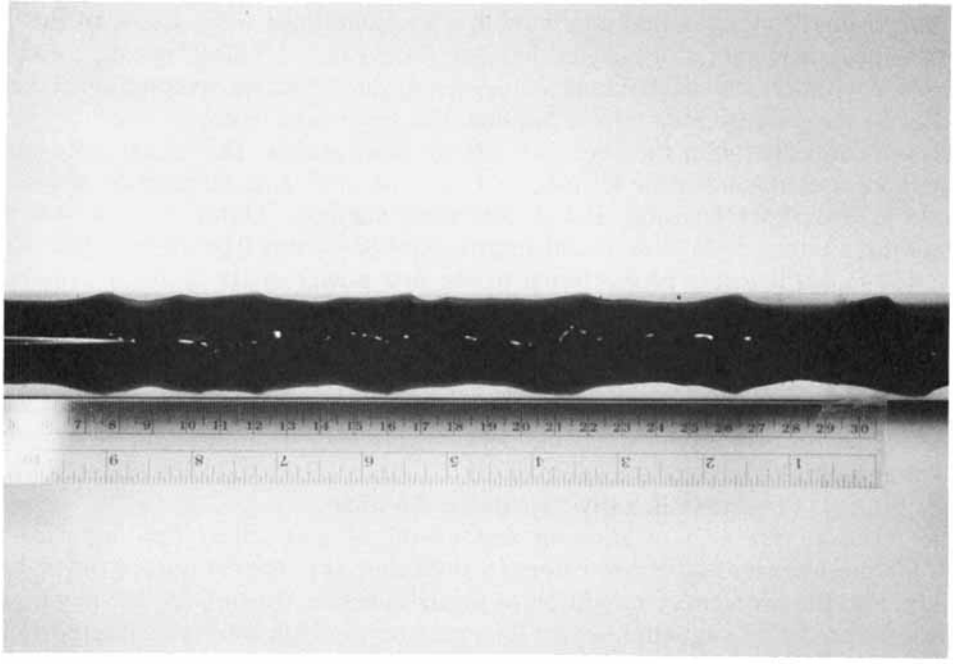

FIGURE 23. The saw-tooth waves on the oil core in a horizontal pipeline. The flow is from left to right. The oil is lighter than water, and the asymmetric waves on the upper surface give rise to an inertial lift that keeps the core from touching the ceiling of the pipe.

Waves are necessary whether the core is levitated by lubrication forces proportional to U or by lift forces proportional to U^2. In experiments and in the field, the core flows are never strictly periodic in the direction of flow, but a definite wavelength can usually be determined. The wave form in a single 'wavelength' is not symmetric and the nature of asymmetry is related to the mechanism of levitation. The kind of asymmetric wave forms which are seen in practice are compatible with the inertial form of lift and not with lubrication. In figure 22, we compare the saw-toothed waves that might be expected (*a*) from the theory of hydrodynamic lubrication and (*b*) from the theory of

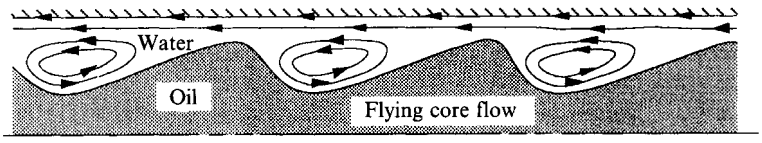

FIGURE 24. Secondary motions in the troughs of the waves shown in figures 22(*b*) and 23 in a coordinate system in which the core is at rest and the pipe moves to left.

aerodynamic lift. The photographs shown in figure 23 show that (*b*) appears to be the configuration one finds in practice. These shapes are even evident in mild form in the bamboo waves which develop in vertical flows where levitation is not an issue, but free surface distortion is (Bai, Chen & Joseph 1992; Joseph & Renardy 1993).

The waves required by lubrication theory look like a slipper bearing in which the gentle ramp moves forward in the water, wedging water between the wall of the pipe and the wave on the core. The flow does not block anywhere so that the steep part of the crest is on the lee-side. The inertially dominated wave responds to the high pressure at the crest by deforming the core so that the steep part of the crest forms at the front side of the crest where the pressure is high, as in the photograph shown in figure 23.

The high pressure at the front of the crest of the wave propagating into the water appears to be associated with a dividing streamline and the point of 'viscous' stagnation as in the dynamics of levitation of elliptic capsules shown in figures 6 and 8. A sketch of the secondary motions that this stagnation flow might imply in the case of the core flow is shown in figure 24. The high pressure at stagnation points produces deep troughs. This is why the assumptions required to justify various long wave approaches to the nonlinear dynamics of core flows are not realized in practice.

In the capsule problem, Liu (1982) talks about a micro-lift in which one part of the capsule is off the wall and macro-lift in which the particles are maintained in flight. Micro-lift seems to be allied to the start-up of vertically stratified, static core flow: stagnant light oil resting on the pipe roof or heavy oil on the pipe floor. Lubrication forces could be dominant in the start-up and might play a role in the flight of the oil core.

6. Conclusions

Because the purpose of this paper is to study the hydrodynamic mechanisms in the lift-off and flying of a capsule, some parameters used may be rather different from those encountered in an actual capsule pipeline. Based on the results and analysis presented in this paper, the following conclusions can be drawn within the parameter ranges covered in this study:

(i) The motion of an elliptic capsule in a horizontal channel consists of three stages: initial lift-off, transient oscillations and steady flying.

(ii) The initial lift-off has two distinct patterns. At large liquid velocity, the tail of the capsule lifts off first due to high pressure under the tail caused by inertia. At small liquid velocity, the nose lifts off first because of lubrication and possibly also inertial effects under the nose.

(iii) The transient oscillations are results of the capsule inertia.

(iv) The hydrodynamic mechanism for the steady flying regime is different depending on the elevation of the capsule. If the capsule flies at low elevation, lubrication is the major effect for the lift force; if the capsule flies at high elevation, inertial effect becomes more important. The behaviour of capsules flying at high liquid velocity

agrees qualitatively with the data of Richards (1992). The mechanism of inertial lift seems to apply to the levitation of heavy cores of crude oil in water-lubricated pipelines.

(v) A capsule of zero buoyant weight stabilizes slightly off the centreline with a small tilt angle. The perfectly symmetric configuration with the capsule lying horizontal on the centreline is not stable.

This work was supported by the NSF, Fluid, Particulate and Hydraulic Systems, by the US Army, Mathematics and AHPCRC, by the DOE, Department of Basic Energy Sciences and the Minnesota Supercomputer Institute and by the Schlumberger Foundation. J.F. was supported in part by a Doctoral Dissertation Fellowship from the Graduate School, University of Minnesota. The authors thank Mr R. Bai for his assistance in preparing the graphics in §5.

REFERENCES

Bai, R., Chen, K. & Joseph, D. D. 1992 Lubricated pipelining: stability of core–annular flow. Part V. Experiments and comparison with theory. *J. Fluid Mech.* **240**, 97–132.

Batchelor, G. K. 1988 *An Introduction to Fluid Dynamics.* Cambridge University Press.

Brown, R. A. S. 1987 Capsule pipeline research at the Alberta Research Council, 1958–1978. *J. Pipelines* **6**, 75–82.

Crochet, M. J., Debaut, B., Keunings, R. & Marchal, J. M. 1991 A finite element program for modeling processes. In *CAE for Polymer Processing: Application in Extrusion and Other Continuous Processes* (ed. K. T. O'Brien). Munchen: Hanser Verlag.

Durlofsky, L., Brady, J. F. & Bossis, G. 1987 Dynamic simulation of hydrodynamically interacting particles. *J. Fluid Mech.* **180**, 21–49.

Ellis, H. S. 1964 The pipeline flow of capsules. Part 4: An experimental investigation of the transport in water of single cylindrical 'capsules' with density greater than that of water. *Can. J. Chem. Engng* **42**, 69–76.

Ellis, H. S. 1976 An analysis of the lift-off of pipeline capsules. *Hydrotransport* **4**, C1-1.

Ellis, H. S. & Kruyer, J. 1970 The pipeline flow of capsules. Part 10. Empirical pressure and velocity correlations for cylindrical capsules conveyed in pipelines up to 4 inches in diameter. *Hydrotransport* **1**, C2–29.

Feng, J., Hu, H. H. & Joseph, D. D. 1994*a* Direct simulation of initial value problems for the motion of solid bodies in a Newtonian fluid. Part 1. Sedimentation. *J. Fluid Mech.* **261**, 95–134.

Feng, J., Hu, H. H. & Joseph, D. D. 1994*b* Direct simulation of initial value problems for the motion of solid bodies in a Newtonian fluid. Part 2. Couette and Poiseuille flows. *J. Fluid Mech.* **277**, 271–301.

Ganatos, P., Pfeffer, R. & Weinbaum, S. 1978 A numerical-solution technique for three-dimensional Stokes flows, with application to the motion of strongly interacting spheres in a plane. *J. Fluid Mech.* **84**, 79–111.

Garg, V. K. 1977 Capsule pipelining – an improved theoretical analysis. *Trans. ASME* I: *J. Fluids Engng* **99**, 763–771.

Govier, G. W. & Aziz, K. 1972 *The Flow of Complex Mixtures in Pipes*, chap. 12. Van Nostrand-Reinhold.

Hesla, T. I., Huang, A. Y. & Joseph, D. D. 1993 A note on the net force and moment on a drop due to surface forces. *J. Colloid Interface Sci.* **158**, 255–257.

Hodgson, G. W. & Charles, M. E. 1963 The pipeline flow of capsules. Part 1: The concept of capsule pipelining. *Can. J. Chem. Engng* **41**, 43–45.

Hu, H. H., Joseph, D. D. & Crochet, M. J. 1992 Direct simulation of fluid particle motions. *Theor. Comput. Fluid Dyn.* **3**, 285–306.

Huang, P. Y., Feng, J. & Joseph, D. D. 1994 The turning couples on an elliptic particle settling in a vertical channel. *J. Fluid Mech.* **271**, 1–16.

HUANG, A. Y. & JOSEPH, D. D. 1995 Stability of eccentric core–annular flow. *J. Fluid Mech.* **282**, 233–245.

JOSEPH, D. D. & RENARDY, Y. Y. 1993 *Fundamentals of Two-Fluid Dynamics. Part II: Lubricated Transport, Drops and Miscible Liquids.* Springer.

KRUYER, J., REDBERGER, P. J. & ELLIS, H. S. 1967 The pipeline flow of capsules. Part 9. *J. Fluid Mech.* **30**, 513–531.

LAZARUS, J. H. & KILNER, F. A. 1970 Incipient motion of solid capsules in pipelines. *Hydrotransport* **1**, C3–45.

LIDDLE, R. T. 1968 A photographic study of capsule behavior in a pipeline. Masters thesis, University of Alberta, Faculty of Graduate Studies.

LIU, H. 1981 Hydraulic capsule pipeline. *J. Pipelines* **1**, 11–23.

LIU, H. 1982 A theory of capsule lift-off in pipeline. *J. Pipelines* **2**, 23–33.

LIU, H. 1992 Design and operational considerations of hydraulic capsule pipelines. Invited lecture at the *Workshop on Capsule Pipelines, Tokyo, Japan. June 22–23, 1992.*

LIU, H. & GRAZE, H. R. 1983 Lift and drag on stationary capsule in pipeline. *ASCE J. Hydraulic Engng* **109**, 28–47.

OLIEMANS, R. V. A. & OOMS, G. 1986 Core-annular flow of oil and water through a pipeline. In *Multiphase Science and Technology*, vol. 2 (ed. G. F. Hewitt, J. M. Delhaye & N. Zuber). Hemisphere.

OLIEMANS, R. V. A., OOMS, G., WU, H. L. & DUYVESTIN, A. 1985 Core-annular oil/water flow: the turbulent-lubricating model and measurements in a 2 in. pipe loop. Presented at the *Middle East Oil Technical Conf. and Exhibition, Bahrain, March 11–14, 1985.* Society of Petroleum Engineers.

OOMS, G., SEGAL, A., VAN DER WEES, A. J., MEERHOFF, R. & OLIEMANS, R. V. A. 1984 A theoretical model for core-annular flow of a very viscous oil core and a water annulus through a horizontal pipe. *Intl J. Multiphase Flow* **10**, 41–60.

RICHARDS, J. 1992 Behavior of coal log trains in hydraulic transport through pipe. MS thesis, Department of Civil Engineering, University of Missouri-Columbia.

SUGIHARA-SEKI, M. 1993 The motion of an elliptical cylinder in channel flow at low Reynolds numbers. *J. Fluid Mech.* **257**, 575–596.